Modeling of Crazing in Rubber-toughened Polymers with LS-DYNA®

M. Helbig, A. Haufe
DYNAmore GmbH, Industriestrasse 2, 70569 Stuttgart, Germany

Abstract

Rubber-toughened polymers such as acrylonitrile butadiene styrene (ABS) or high-impact polystyrene (HIPS) are composed of a thermoplastic matrix and small rubber particles, e.g. [1]. The enhanced fracture toughness and ductility, compared to the neat matrix material, are the advantages of rubber-toughened polymers [2]. These macroscopic effects are caused by mechanisms on the micro scale such as shear yielding, void growth and crazing. Crazing is understood as the formation of localized zones of fibrillated material which are able to transfer load. Stress whitening in combination with an increasing volumetric strain clearly indicates the crazing mechanism. The macroscopic volume typically stays constant during shear yielding. The yield and deformation behavior of a rubber-toughened polymer was characterized at the laboratory of DYNAmore GmbH, Stuttgart. For modeling of the dilatant deformation behavior MAT_SAMP-1 was used. Damage modelling depending on the deformation mechanism (shear yielding or crazing) can be taken into account via eGISSMO (i.e. *MAT_ADD_GENERALIZED_DAMAGE).

Introduction

Rubber toughened polymers such as ABS or HIPS are widely used in technical products e.g. bumpers, mobile phones, domestic appliances or toys. Toughness and ductility of neat thermoplastic polymers styrene acrylonitrile resin (SAN) or polystyrene (PS) can be improved with fine dispersed rubber particles. These rubber particles initiate microscale deformation mechanisms such as shear yielding or crazing of the matrix phase by void growth. The interrelation of the mechanisms depends on the rubber particle size, the void volume fraction of the particles, the loading rate, the stress triaxiality and the matrix material, e.g. [3, 4, 5, 6 or 7]. Crazing and the interaction with shear yielding are on the particular interest of this work.
Crazing is the formation of localized zones in which the bulk polymer is drawn into thin fibrils [8]. In homogeneous polymers crazing is a precursor of brittle failure under tensile load. In rubber toughened polymers crazing occurs between the rubber particles, see [2, 3], also known as distributed crazing. In HIPS most of the deformation and damage occurs due to crazing. In toughened polymers with more ductile matrix behavior, such as ABS, crazing and shear yielding can be observed simultaneously. Increasing volume with increasing inelastic deformation under uniaxial tensile load and stress whitening can be seen as indicators of crazing where constant volume, necking and shear bands with increasing tensile load are typically indicators of the shear yield mechanism. The interaction of different yield and damage mechanisms are subject of different investigations, e.g. [10, 11, 12]. Due to unknown micro structure (e.g. particle volume fraction or size of rubber particles) and therefore unknown constitutive properties the usage of phenomenological material models is state of the art. In this paper some important combinations of material and damage models of LS-DYNA are shown. Most of the experiments in this paper were performed at DYNAmore, Stuttgart, Germany.

Experimental results

A tensile testing machine with a capacity up to 100kN and the maximal loading speed of 3.3 mm/s was used for the quasi-static tests. Quasi-static tensile, bending, compression and biaxial punch tests can be done with the testing equipment at DYNAmore. The strains were determined with a 3D-optical, local displacement measurement system, which captures the displacements of speckle patterns by two cameras via DIC, see Figure 1, right. The DIC system captures the deformation with up to 15 Hz. For the quasi-static tensile tests a modified DIN EN ISO D527 tensile specimen was used as depicted in Figure 1, left. The width was expanded to 6.0 mm, such that for calibration reasons three linear finite elements with 2 mm edge length could be used for the simulation I reverse engineering. The loading speed was 0.03 mm/s, therefore a nominal strain rate of 0.001 1/s was reached.

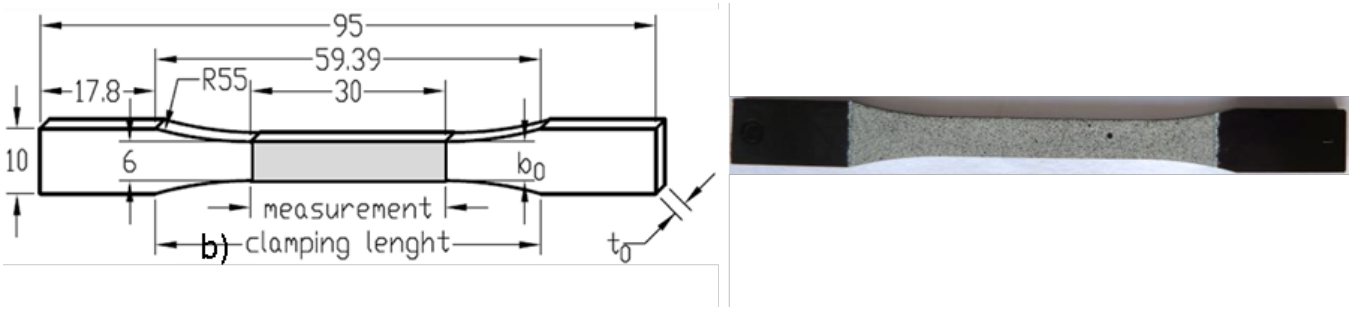

Figure 1: Geometry of the tensile specimen and coupon with speckle pattern for DIC strain measurement

The stress vs. strain curves of the quasi-static tensile tests of a PC/ABS are shown on the left in Figure 2. The clamping length is about 60 mm and the engineering strain is based on 30mm measuring length. On the right of

Figure 2 the contour plots of the logarithmic major strain at different deformation stages are shown. The letters (a...e) connect the contour plots of the logarithmic major strain to the engineering stress-strain curve.

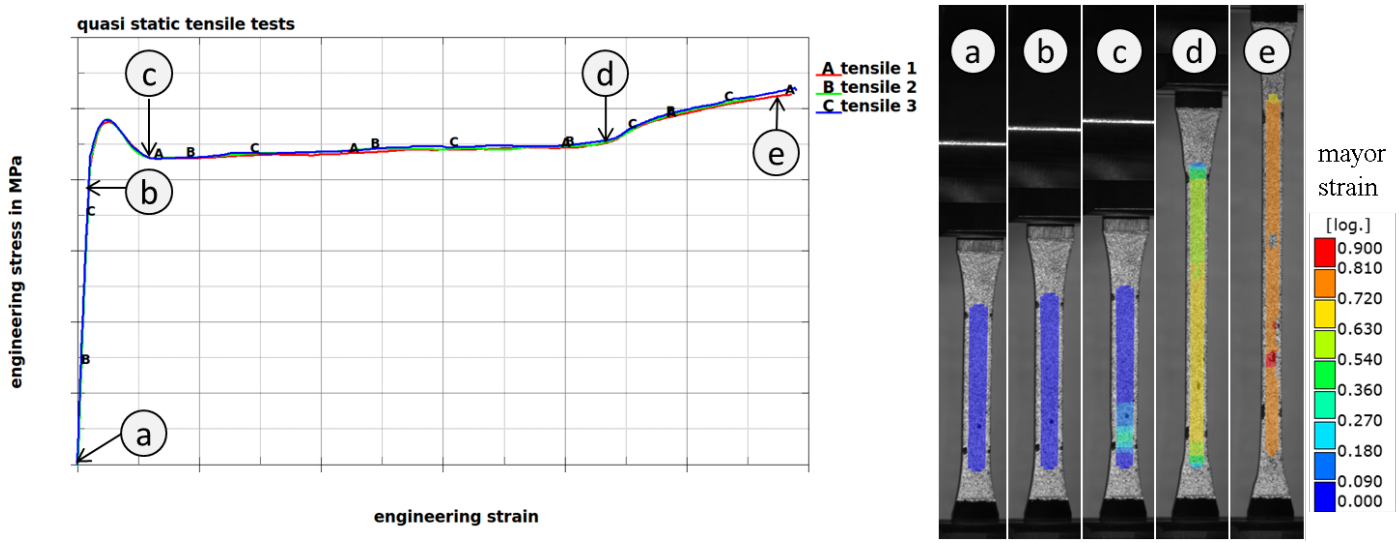

Figure 2: Stress-strain curves of quasi static tensile tests and contour plots of major strain at different deformation stages

Point *a* in Figure 2 shows the unloaded specimen. Point *b* indicates the end of the elastic deformation before yielding starts. At the beginning of yielding the stress increases until a local maximum value is reached. Then softening can be overserved in the engineering stress-strain curve until a local minimum is reached, see point *c*, where necking starts. Necking increases until the parallel cross section is fully stretched, see point *d*. The final kink in the engineering stress vs. strain curve can be attributed to the growth of the necking area into the non-parallel section until a critical stretch is reached and the specimen fails eventually.

As stated before, the volumetric strain can be seen as an indicator of crazing. Therefore the logarithmic strain in loading direction and perpendicular to the loading direction at a local area of 6mm x 2mm is used, as shown in red color in Figure 3. The volumetric strain is defined as the sum of the logarithmic (Hencky) strains:

$$\varepsilon_v^H = \varepsilon_{xx}^H + \varepsilon_{yy}^H + \varepsilon_{zz}^H = \varepsilon_{xx}^H + 2\,\varepsilon_{yy}^H$$

With the assumption, straining in thickness (z-direction) to be equal to straining in width (y-direction) volumetric strain can be determined directly from DIC data, as shown in Figure 3 for three different tests.

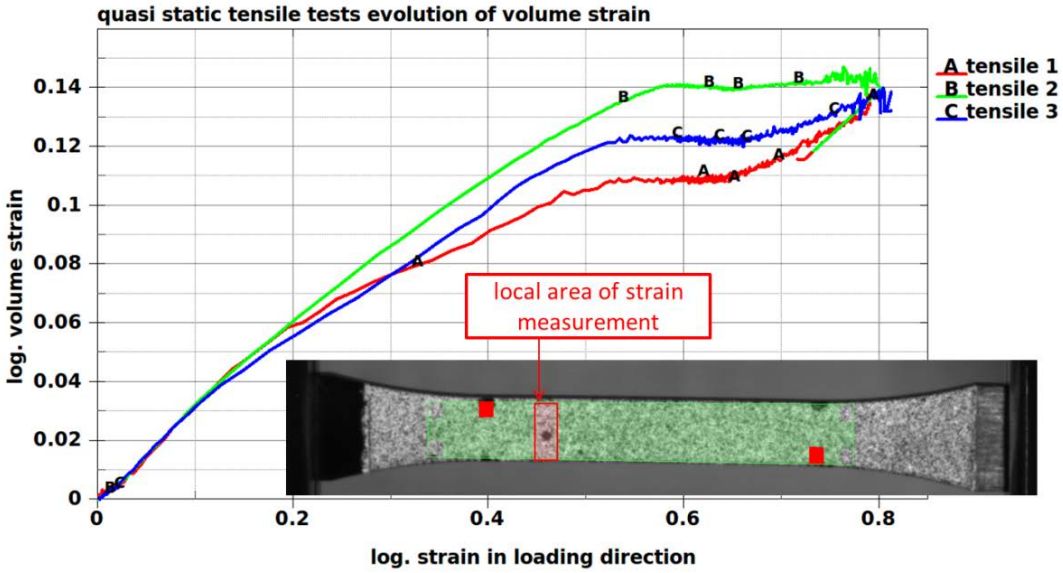

Figure 3: Evolution of volumetric strain measured local area of 6mm x 2mm

The graph in Figure 3 shows that the volume increases with increasing deformation. Therefore the assumption of pure shear yielding as sole deformation and damage mechanism does not hold. Hence crazing should be taken into account as well. Compared to a neat ABS specimen, see [2], where the volumetric strain reaches a level of about 0.4, the volume increase of the tested PC/ABS is rather small. Furthermore it depends very much on the composition of the material as well, e.g. [11, 13].
For the tensile tests a nominal strain rate $\dot{\varepsilon} = v/l_0$ is defined as loading speed v divided by the initial length $l_0 = 30$mm. The strain rate dependency of the material investigated for four decades is shown in Figure 4 (nominal strain rate depicted).

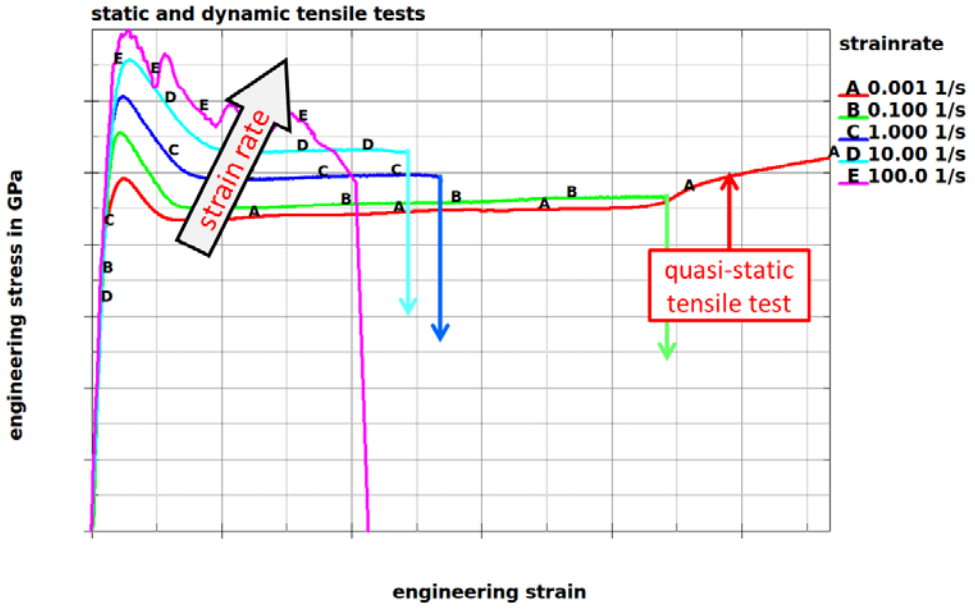

Figure 4: Quasi static and dynamic tensile tests

With increasing loading speed the stress level for plastic deformations increases and the engineering strain at failure decreases. Additionally three point bending tests were performed at the laboratory of DYNAmore in Stuttgart, Germany. A *4a impetus* pendulum, see [15], was used for these test setups. The pendulum is designed for fast and easy dynamic tests of polymers, foams and composite materials. The arm of the pendulum is fiexed at a certain angle and stores the potential energy $W_{pot} = mgh$. At the start of the test the lever is released and the pendulum hits the specimen with the kinetic energy of $W_{kin} = 1/2mv_0^2$. If it is assumed, that the potential energy is equal to the kinematic energy, the initial velocity v_0 is independent of mass m and only depends on the lever height h, i.e. the angle of pendulum arm. In this setup impact velocities from 0.5 up to 4.3m/s can be used. The nominal strain rate $\dot{\varepsilon} = 6vt/l_w^2$ depends on the impact velocity v, the thickness t and the measuring length l_w. The specimens used for the characterization tests are shown in Figure 5.

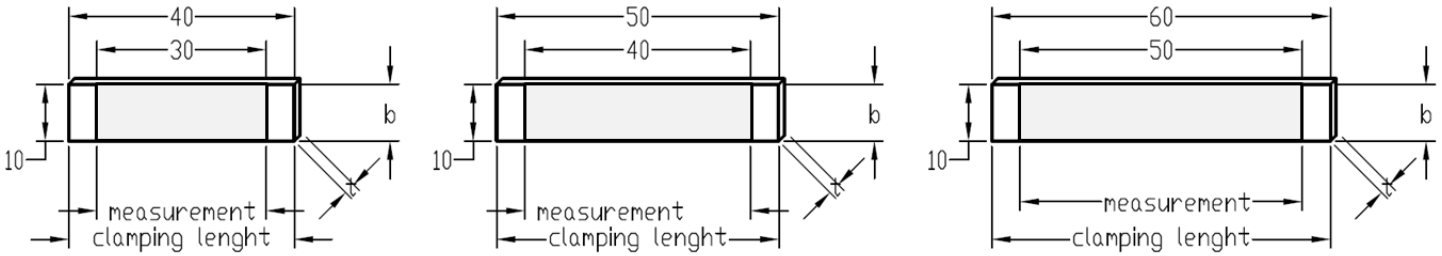

Figure 5: Specimen for dynamic three point bending

The thickness of the coupons was 2.0 mm. Hence a maximal strain rate of 57.3/s is being reached. Figure 6 shows the strain rate as function of the engineering strain for these three point bending tests.

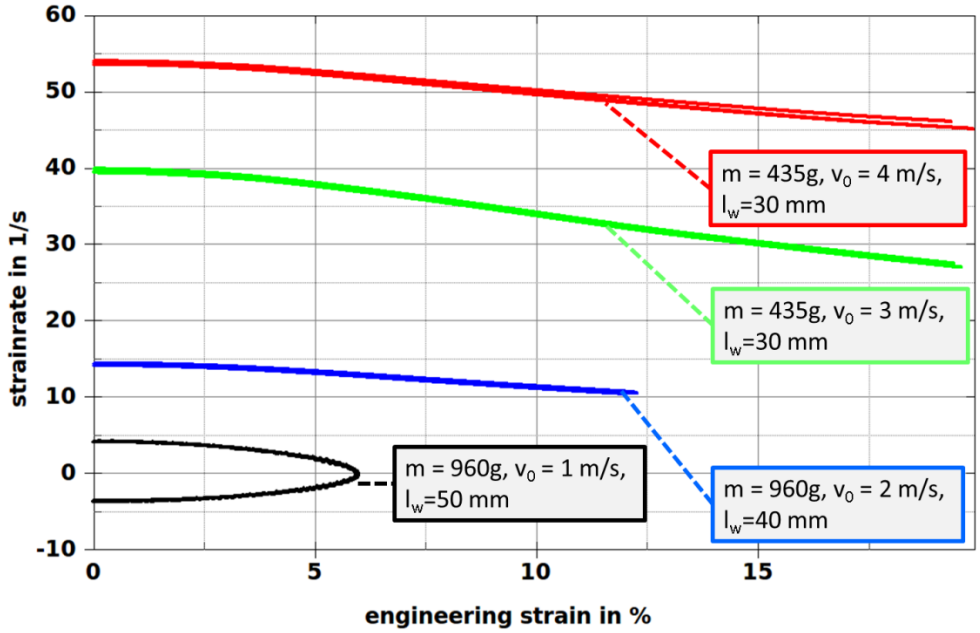

Figure 6: Strain rate vs. engineering strain of dynamic three point bending tests

With three different specimens as depicted in Figure 5 dynamic bending tests were performed. To increase the kinetic energy additional mass may be fixed at top of pendulum arm. For the tests with nominal velocity of 1.0m/s and 2.0m/s such additional mass was added to the arm. Nevertheless the specimens have shown significant ductility in this loading scenario and did not break.
The engineering stress vs. engineering strain curves for all dynamic bending tests are shown in Figure 7.

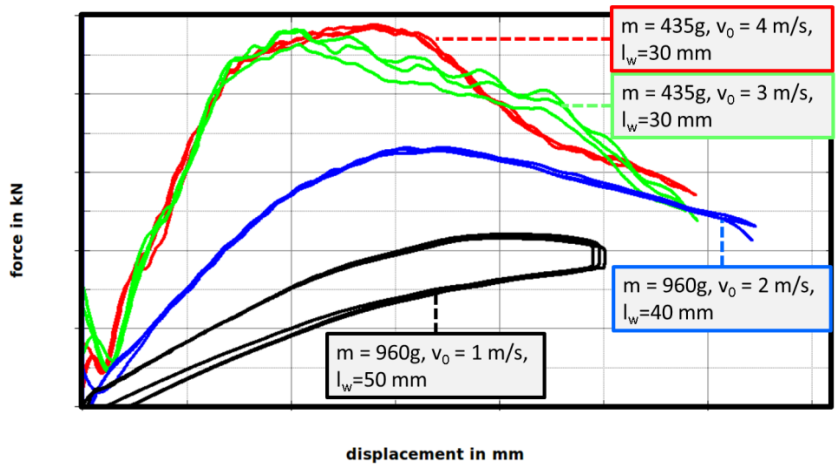

Figure 7: Force vs. displacement of dynamic three point bending tests

No clear difference between the two fastest tests can be overserved. Figure 7 indicates that the force level for these two tests differ only slightly. For the tensile tests a similar trend can be anticipated. A possible explanation may be adiabatic heating, which is observed in several thermoplastic materials.

Material parameter identification

It is recommended to start with a basic constitutive model that captures the major effects of the investigated material. Therefore *MAT_PIECEWISE_LINEAR_PLASTICITY (*MAT_024) was chose at first. It needs to be noted that the underlying von Mises plasticity model assumes isochoric behavior in plastic loading and hence may not only be accurate in certain regions of the loading history. The beginning of the yield curve can be directly determined from the engineering stress vs. strain curve. Figure 8 shows three different true stress vs. true strain curves with the formulas used to generate the curves (loading direction denoted as *x*).
For the red curve #1 in Figure 8 the engineering stress vs. engineering strain curves are used. Here the strain is measured between two points on the coupon with a distance of 30 mm. Here constant volume is assumed for the computation of the true stress values. In the green curve #2 the local logarithmic strain was used to compute the true stress and the strain was determined locally. As can be observed in Figure 8 the missing softening behavior is the most important difference between curve #1 and curve #2. This can be attributed to the local strain measurement. Curve #3 (blue) of Figure 8 shows a true stress vs. true strain curve which was determined by using the local straining in loading and width direction. Here was assumed that the strain in both perpendicular directions is equal. Determination of Young's modulus is done by fitting a linear equation to the experimental results as shown in Figure 9.

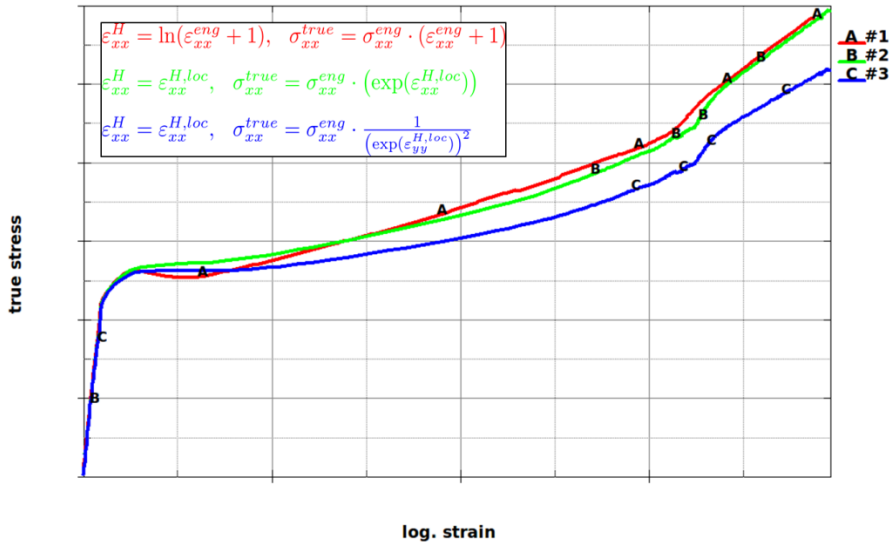

Figure 8: Different evaluation of true stress vs. logarithmic strain curves

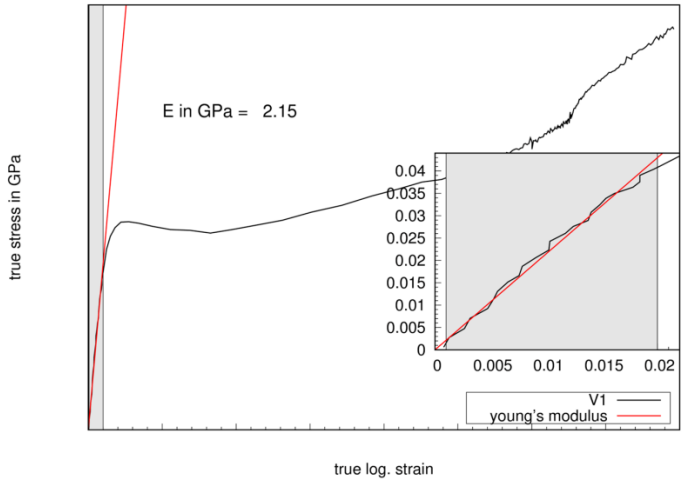

Figure 9: Determination of Young's modulus

A modulus of 2.15GPa was found which corresponds well to values from the literature and the granulate manufacturer [9]. The domain of plastic deformation can now be determined by subtracting the elastic deformation from the total logarithmic strains ε^{tot}. Figure 10 shows the yield curves w.r.t. the plastic strain component $\varepsilon^{pl} = \varepsilon^{tot} - \sigma/E$. The colors of the yield curves in Figure 10 correspond to Figure 8.

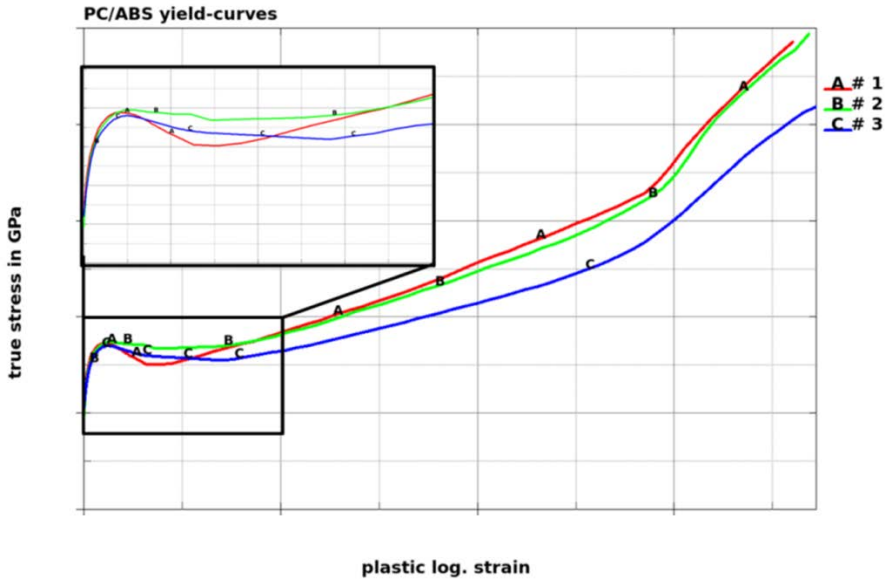

Figure 10: Yield curves determined from experimental data

All curves exhibit softening behavior at different plastic straining past an initial peak. Also the stress level at the beginning of the inelastic deformation varies and the re-hardening at large plastic deformations differs clearly.

Modelling and simulation of coupon tests

The parameters for two different constitutive models were determined by a reverse engineering optimization strategy, i.e. the parameters were determined by simulation of the coupon tests and comparison with the experimental results. Fully integrated, linear shell elements (ELFORM=16) and solid elements (ELFORM=-1) are used for the comparison between simulation and experiment data. The finite element tension models are depicted on the left of Figure 11.

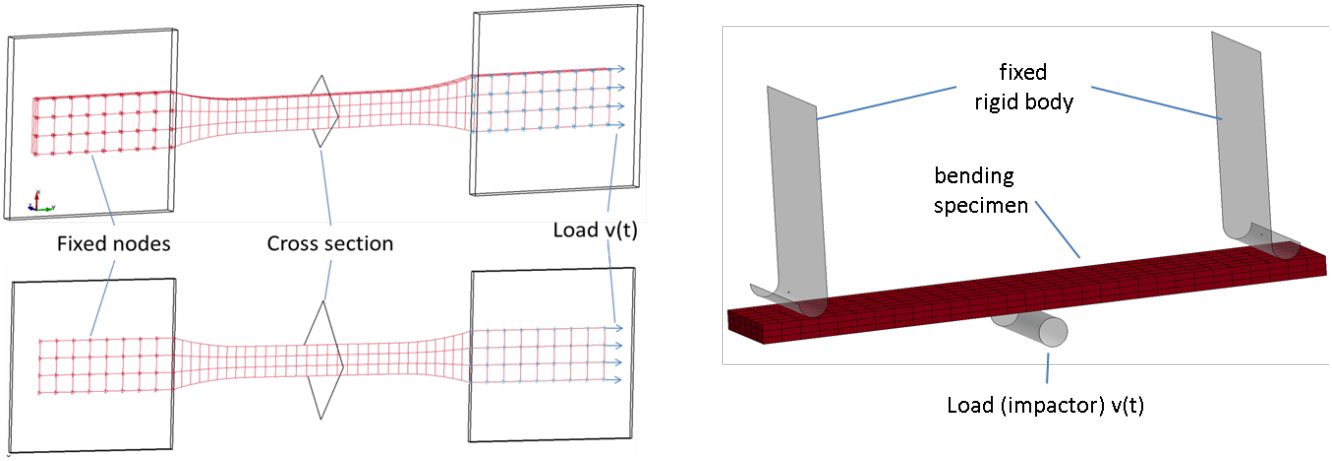

Figure 11: Finite element model of tensile and bending tests

For boundary definition box definitions were used and a cross section was defined in the center of the specimen. Constant velocity in y-direction is applied. For the dynamic three point bending tests the corresponding finite element models as well as the loading and boundary conditions were generated automatically within the 4a Impetus software [15]. An example of the latter is depicted to the right in Figure 11.
As a first try a tensile test is simulated by using the yield curves determined directly from the experiments, see Figure 10. The comparison of experiments and simulations is shown in Figure 12.

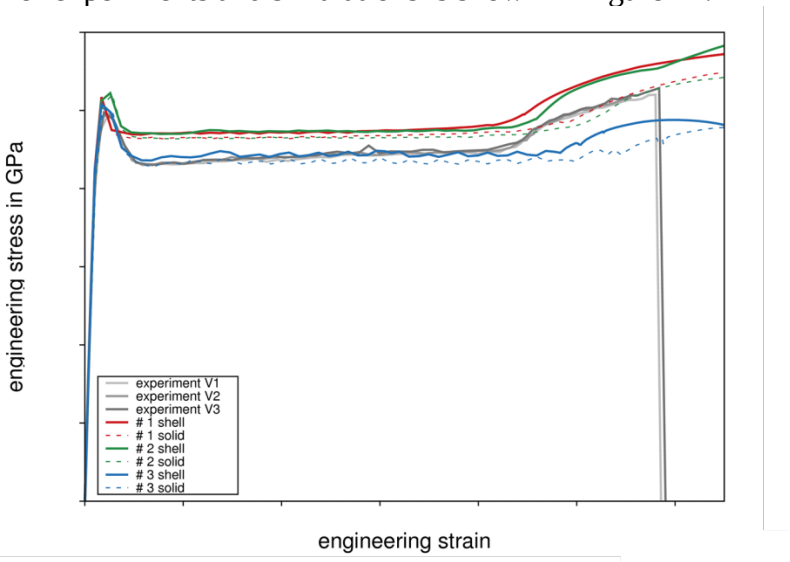

Figure 12: Simulation of tensile tests with experimental data

The simulations with yield curves #1 and #2 overestimate the measured stress level. A clear difference between shell and solid elements can be seen at larger engineering strain ($\varepsilon^{eng} > 0.8$) and can be attributed to the different constitutive models and respective section deformations. The stress level fits quite well to the experiments for the yield curve #3 for lower engineering strain ($\varepsilon^{eng} < 0.8$). A comparison between simulation and experiment of the maximal logarithmic principal strain for different load states is depicted on the right of Figure 13. On the left in Figure 13 the different load states are marked in the engineering stress vs. strain curves. Compared are the experiments and the simulation with solid elements and yield curve #3.

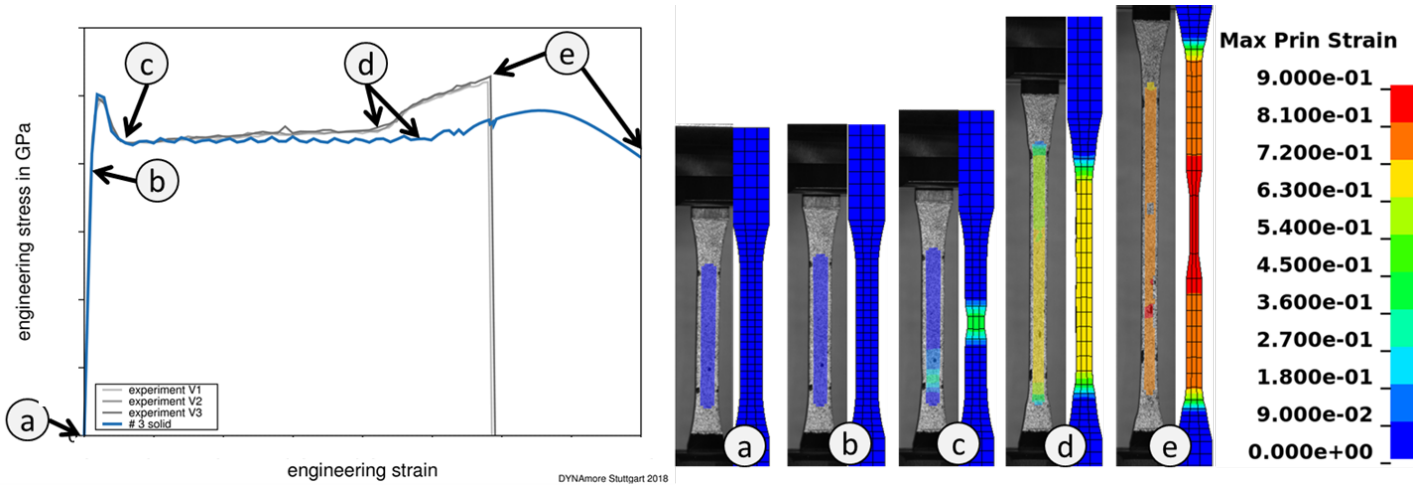

Figure 13: Comparison of simulation vs. experiments: stress vs. strain curves and contour plot of major strain

A good agreement between experiment and simulation is experienced for small strains ($\varepsilon^{eng} < 0.3$). With increasing deformation the stress level of the simulation does not increase enough compared to the experiments.

One reason for this deviation may be the decreasing slope of in the yield curve at higher strains ($\varepsilon^{pl} > 0.7$), see blue curve in Figure 10. Another explanation can be found by the discretization with solid elements, see difference between blue curves in Figure 12. Nevertheless, for this simple and fast way of converting experimental data to a yield curve the agreement is reasonably well.

However, in some cases it might be necessary to have the yield curve available for very high values of the plastic straining as well. Therefore three parameters of a quadratic polynomial equation were determined by a smooth curve fitting, as shown in the left of Figure 14. On the right of Figure 14 the updated extrapolated yield curve is shown.

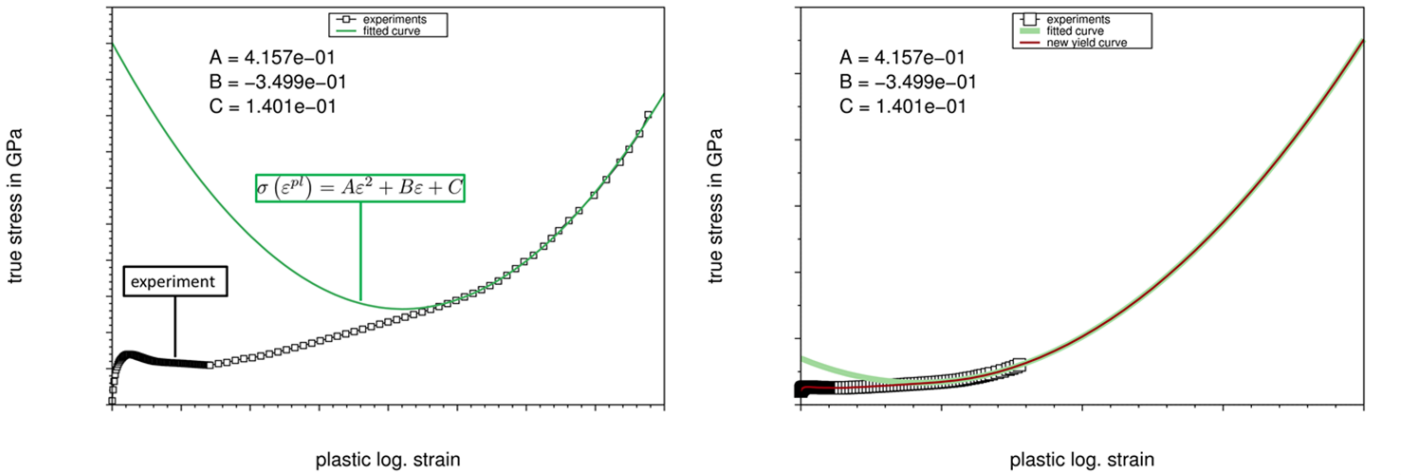

Figure 14: Extrapolation via polynomial function

Strain rate dependency of yield and damage behavior

For rubber-modified thermoplastics strain rate dependency in yield and damage behavior has to be considered. Here again MAT_024 and a shifted yield curve (see Figure 15) is applied until an acceptable deviation to the dynamic tensile tests could be achieved, as shown in Figure 17.

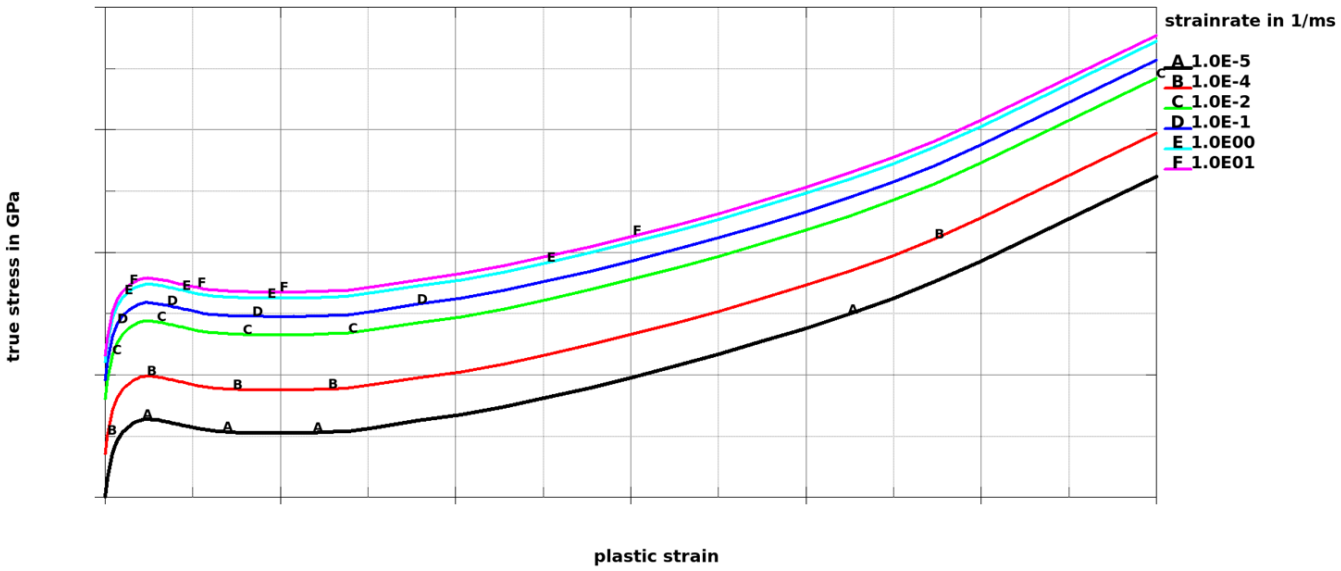

Figure 15: Yield curves for visco-plastic behavior

To consider the strain rate dependency in the event of fracture MAT_ADD_EROSION (GISSMO) was applied. Figure 16 shows that the fracture strain decreases with increasing strain rate until a strain rate of $\dot{\varepsilon} = 0.1\ 1/ms$.

Further on in strain rate direction the values increase dramatically. This may be due to the dynamic tensile test data used where the strain was not measured locally with DIC. Another explanation may be a change in the occurring damage mechanism or adiabatic heating of the specimen. For the available dynamic tests it was not possible to determine the strain perpendicular to the loading direction.

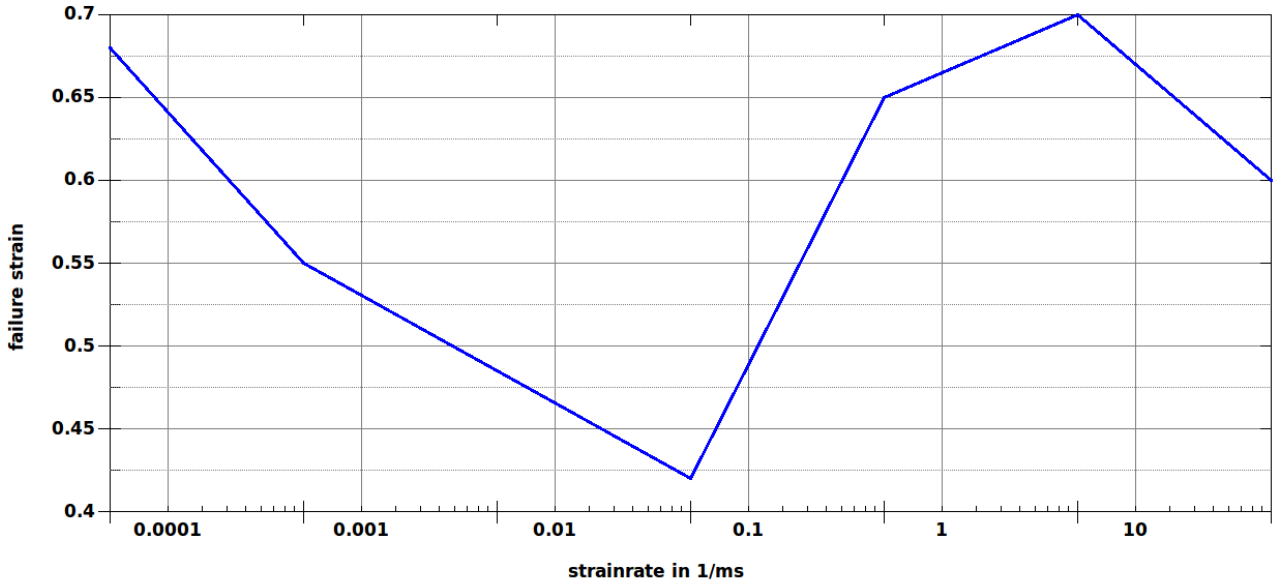

Figure 16: Strain rate dependent fracture strain

In Figure 17 the calibration results of quasi-static and dynamic tensile tests is shown for five different loading rates. Fracture parameters are adjusted according to the available experimental data, such that acceptable agreement between simulation and experiment is achieved.

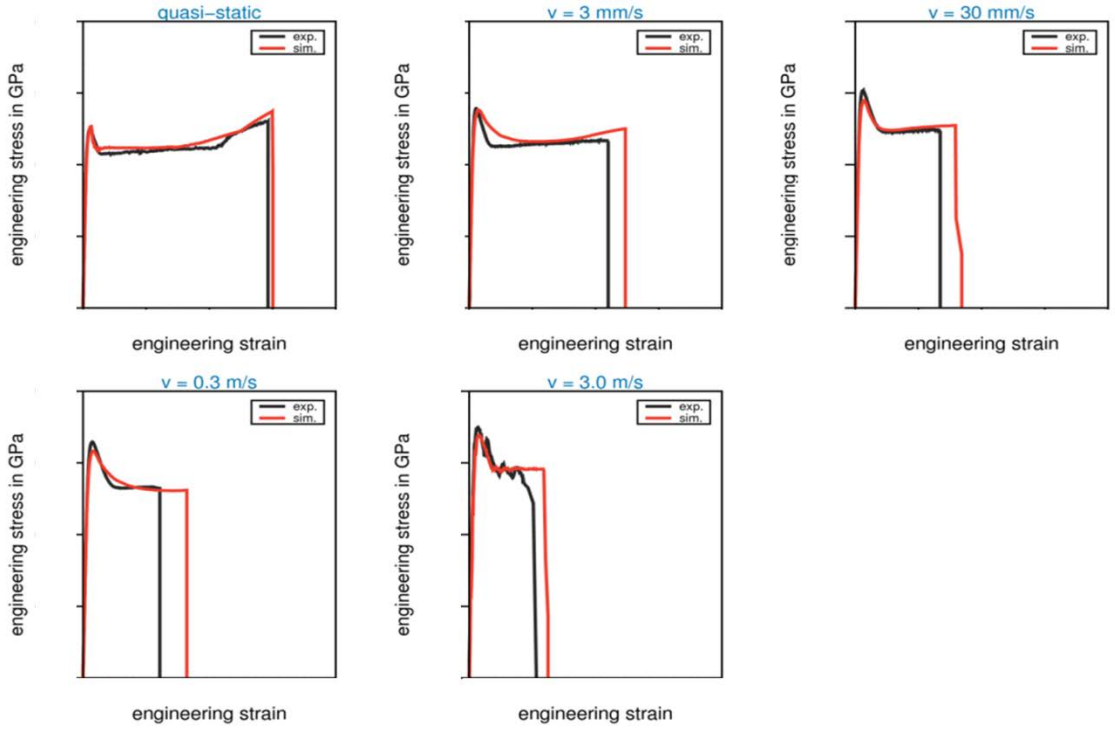

Figure 17: Calibration results of strain rate dependency in tensile specimen

The fracture curve (i.e. element erosion based on accumulated equivalent plastic strain as function of stress triaxility) is assumed to be constant w.r.t. the stress triaxiality in all simulations. The comparison of the dynamic bending experiments and the simulation shows an acceptable agreement also, compare Figure 18. Good agreement for lower strain rates (blue and black curves) is achieved. For higher strain rates the calibrated model overestimates the force level. Due to the ductile behavior the bending specimens did not break in the pendulum tests. Hence damage could not be adjusted under this load.

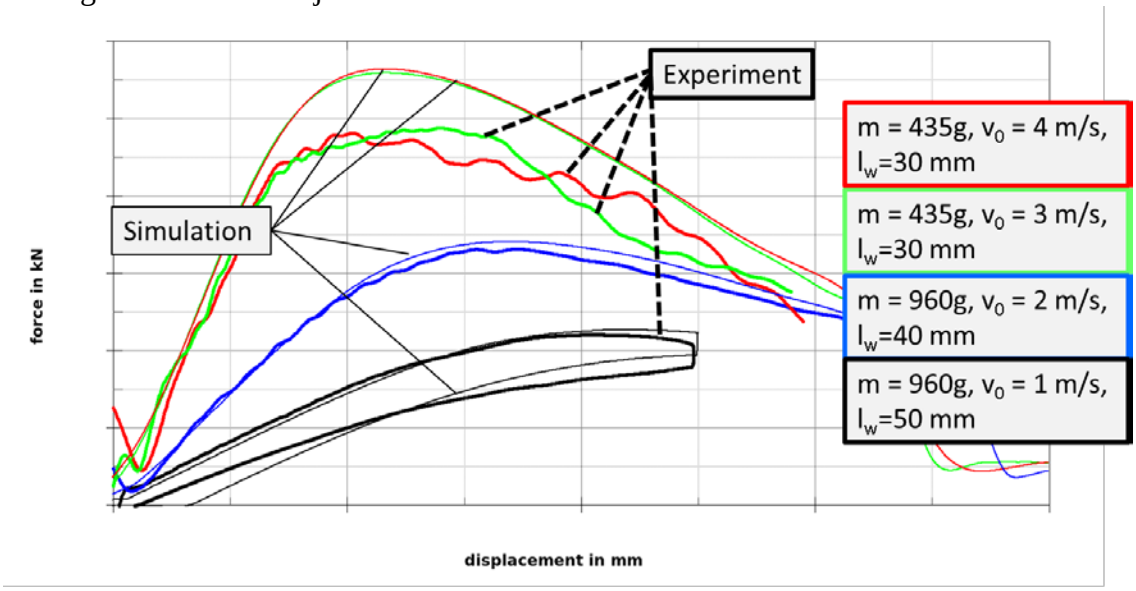

Figure 18: Comparison of dynamic bending tests and adjusted material

Enhanced modelling of polymers using SAMP-1

For simulation with the **S**emi-**A**nalytical **M**odel for **P**olymers-model (SAMP-1) the parameters from *MAT_024 were used in a first step. In case the plastic Poisson's ratio is set to 0.5 and only a yield curve in tensile direction is defined SAMP-1 delivers identical results as MAT_024 (compare black curve and blue curve in Figure 19).

In a next step the volumetric straining may be taken into account. Therefore the plastic Poisons ratio as a function of the accumulated plastic strain has to be defined. Typically use of data from DIC is being made to generate a corresponding curve. In the following a one element test was used to determine the curve via comparison of the measured and the computed volumetric strain. As an advantage of this approach the elastic part of the volumetric strain has not to be separated. On the left of Figure 20 the volumetric strain $\varepsilon_{vol} = \sum \varepsilon_{ii}^{H}$ as sum of the Hencky strains in three directions as a function of the true strain in loading direction is shown. Here the black curve shows an experimental curve of a tensile test. The green and black dotted curves show the evolution of the volumetric strain of a non-dilatant material (MAT_024 or MAT_187 with plastic Poisson's ratio of 0.5). The blue curve shows the increase of the volumetric strain for plastic Poisson's ratio of 0.0 (i.e. only crazing occurs). In real rubber toughened materials booth mechanisms, namely shear yielding and crazing, interact depending on the stress triaxiality or the applied strain rate. The volume increase shown in the read curve is the result of a plastic Poisson's ratio shown on the right of Figure 20.

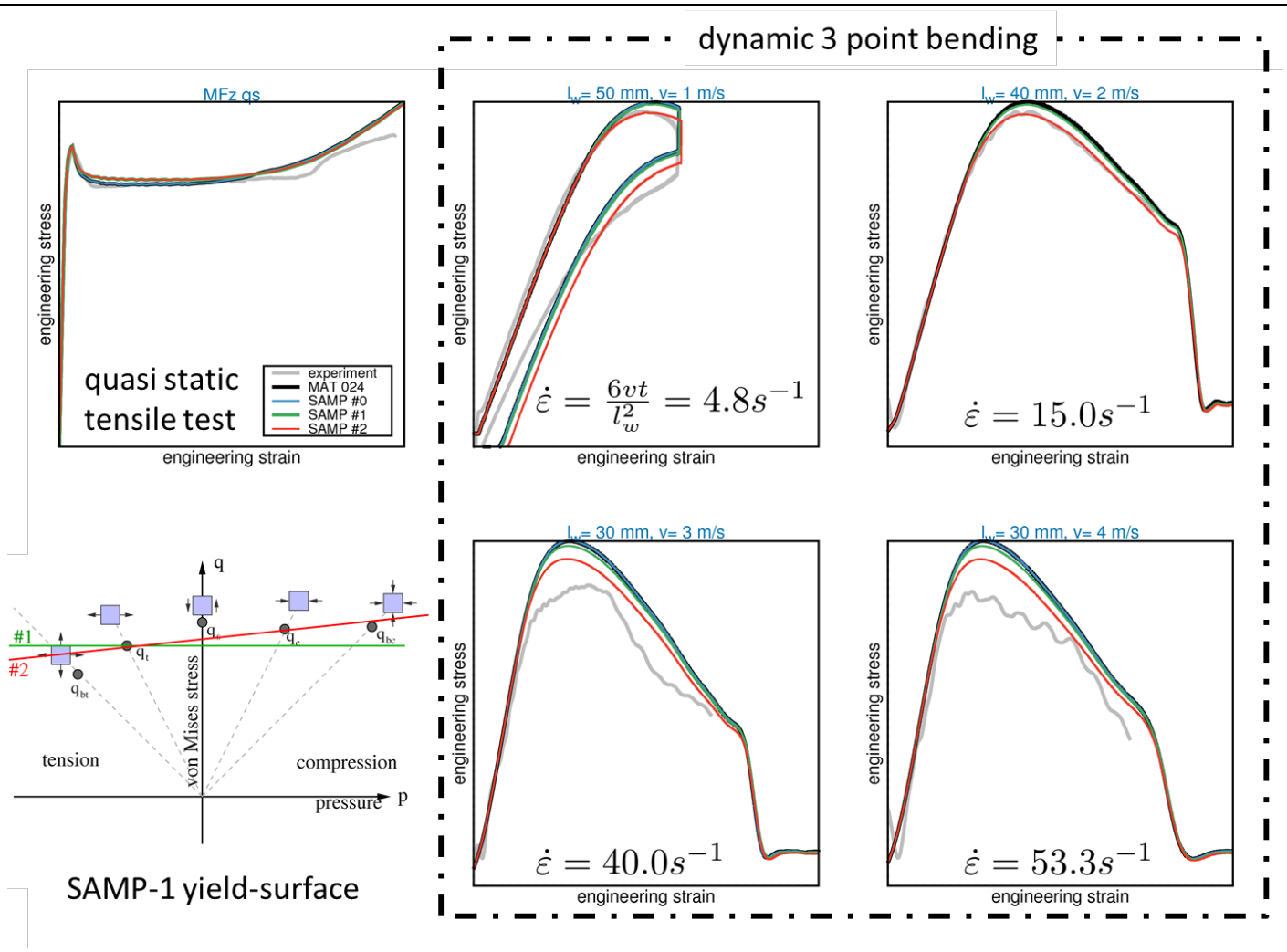

Figure 19: Comparison of experiments to simulation with MAT_024 and MAT_187

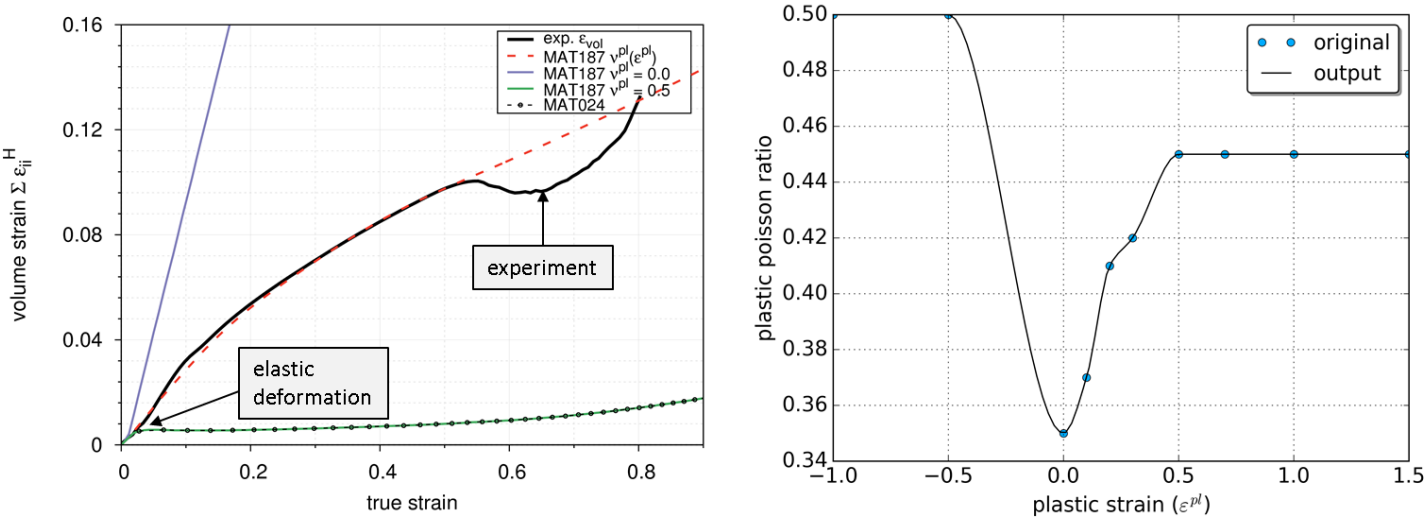

Figure 20: Consideration of dilatant material behavior with the help of plastic transverse contraction

For the non-dilatant constitutive behavior SAMP-1 results in a non-associated flow rule. Therefore the increment of the accumulated plastic strain is now also depended on the flow direction in hydrostatic direction.

The yield curve, which was applied with MAT_024, must therefore be modified to achieve an agreement between the engineering stress vs. strain curves of the experiments and the simulations of the coupon tests.
The results of taking the plastic Poisson's ratio into account is shown in green (curve #1) Figure 20. With smooth scaling operations the same quality of agreement between experiments and simulations are achieved. The difference between simulation with MAT_187 with a plastic Poisson ratio as a function of the accumulated plastic strain and MAT_024 is shown in Figure 21. Two tensile tests at the same load state are shown. The simulation with MAT_024 shows a higher true strain perpendicular to the loading direction.

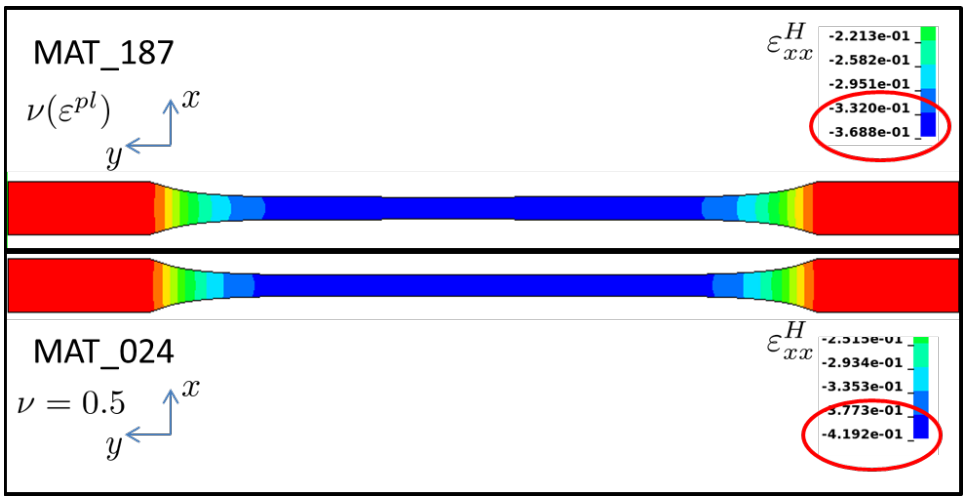

Figure 21: MAT_024 vs. MAT_187 strain perpendicular to loading direction

The results under compression can be improved by taking the inelastic deformation behavior under compression loading into account. Due to the lack of respective data the tensile yield curve was used instead but scaled accordingly. The results of the bending simulations are improved by taking the compression behavior into account. The advantage of SAMP vs. a Drucker-Prager model can be seen in the fact that volume expansion can be taken into account.

Enhanced failure modelling with eGISSMO

Modelling of damage behavior is an important topic since the beginning of finite element simulation. In the last decade modelling the evolution of damage depending on stress triaxiality and eventually eroding of elements was becoming state of the art. Therefore the **G**eneralized **I**ncremental **S**tress-**S**tate dependent **D**amage **Mo**del (GISSMO) is widely applied. In combination with SAMP-1 damage can now be defined as a function of the volumetric strain or any other history variable. An enhancement of the GISSMO model [16] that allows anisotropic damage modelling or alternatively taking up to three different damage driving quantities for almost unrestricted damage modelling into account is now available. As a special case also modelling damage as a function of dilatant and non-dilatant constitutive behavior is possible.
Therefore an **eGISSMO** card for shear yielding as a function of the stress triaxiality and an additional **eGISSMO** card for crazing as a function of the stress triaxiality may be defined, as shown on the left of Figure 22. On the right of Figure 22 the stress triaxiality as function of accumulated plastic strain in different 3D elements (one element tests) is shown. Fracture (eroding) of elements with increasing volume (crazing) can be defined independent of damage growth due to shear yielding.

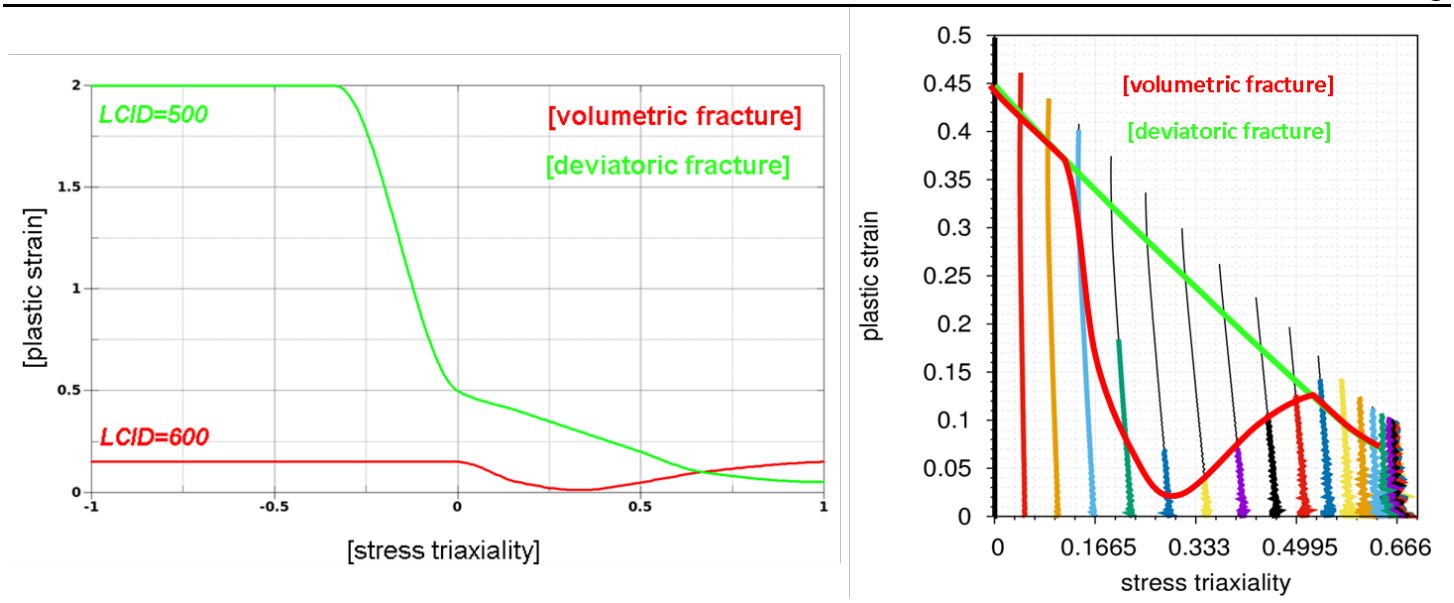

Figure 22: Modelling of dilatant damage using eGISSMO

Summary

Quasi-static tensile tests of a PC/ABS were performed and elastic and inelastic deformation behavior of this material was determined. The straining was measured with a DIC system. Increasing volumetric straining was measured and accounted for as indication of the underlying crazing mechanism. The Young's modulus was determined by fitting a linear function to the stress vs. strain curves of the tensile tests. Dynamic tensile tests and three point bending tests were performed to determinate the strain rate behavior of the material. For the first step the coupon tests were simulated with von Mises plasticity (MAT_024). Determination of the strain rate behavior by reverse engineering for the yield and damage behavior was shown. In a next step the plastic Poisson's ratio was taken into account by using the SAMP-1 material model in order to model and consider the increasing volumetric strain with increasing tensile load. The simulation of bending tests was improved by the consideration of compression-tension asymmetry with the SAMP-1 model.
Finally fracture modelling with increasing volumetric straining with the eGISSMO model was shown.

References

[1] W. Grellmann and S. Seidler (eds.). Deformation and fracture behavior of Polymers (Springer, 2001)

[2] M. Ishikawa, 1995. Stability of plastic deformation and toughness of polycarbonate blended with poly (acrylonitrile-butadiene-styrene) copolymer. Polymer 36, 2203-2210.

[3] M. Helbig, E. van der Giessen, A.H. Clausen, Th. Seelig. Continuum-micromechanical modeling of distributed crazing in rubber-toughened polymers, European Journal of Mechanics - A/Solids, Volume 57, 2016, Pages 108-120.

[4] P. Beahan, A. Thomas and M. Bevis, 1976. Some observations on the micro-morphology of deformed ABS and HIPS rubber-modified materials. J. Mat. Sci. 11, 1207-1214.

[5] C.R. Bernal, P.M. Frontini, M. Sforza and M.A. Bibbo, 1995. Microstructure, deformation and fracture behavior of commercial ABS resins. J. App. Pol. Sci. 58, 1-10.

[6] A.M. Donald and E.J. Kramer, 1982. Plastic deformation mechanisms in poly(acrylonitrile-butadiene styrene) ABS. J. Mat. Sci. 17, 1765-1772.

[7] A. Steenbrink, E. van der Giessen, and P. Wu, 1997. Void growth in glassy polymers. In: Journal of the Mechanics and Physics of Solids, 45 No 3, pp. 405 – 437.

[8] E.J. Kramer and L.L. Berger, 1991. Fundamental processes of craze growth and fracture. In: Kausch, H.H. (Ed.), Crazing in Polymers, Vol. 2. Springer, pp. 1-68.

[9] http://www2.basf.us/businesses/plasticportal/pp_products_campusdownload_en.html

[10] Th. Seelig and E. van der Giessen, 2006. Modeling the interaction of crazing and matrix plasticity in rubber-toughened polymers. In: Meijer HEH (ed), Proceedings of 13th International conference on deformation, yield and fracture of polymers (2006), S. 275–278.

[11] J. Ruge, 2017. Entwicklung eines visko-plastischen Werkstoffmodells für gummimodifizierte thermoplastische Kunststoffe. Master-Thesis, Institut für Mechanik (IFM), Karlsruher Institut für Technologie.

[12] H. Jiang, J. Zhang, Z. Yang, Ch. Jiang and G. Kang,2017. Modeling of competition between shear yielding and crazing in amorphous polymers' scratch, International Journal of Solids and Structures, Volume 124, Pages 21, 5-228.

[13] J. Naumann, 2015. Bruchmechanische Experimente an Kunststoffen unter optischer Verformungsanalyse mittels digitaler Bildkorrelation, Bachelor Thesis, Institut für Mechanik (IFM), Karlsuher Institut für Technologie.

[14] S. Kolling, A. Haufe, M. Feucht and P.A. Du Bois, 2005. SAMP-1: A Semi-Analytical Model for the Simulation of Polymers, 4th German LS-DYNA Anwenderforum, Bamberg.

[15] P. Reithofer, M. Fritz and R. Hafellner, 2009. 4a-impetus - efficient evaluation of material cards for non-reinforced and reinforced thermoplastics, 7th European LS-DYNA Conference.

[16] T. Erhart, P.A. Du Bois and F.Andrade, 2017: Short Introduction of a new Generalized Damage Model, 11th European LS-DYNA Conference 2017, Salzburg, AUT.